

STELLAR OCCULTATIONS AT UV WAVELENGTHS BY THE SPICAM INSTRUMENT: RETRIEVAL AND ANALYSIS OF MARTIAN HAZE PROFILES.

F. Montmessin, J.L. Bertaux, P. Rannou, *Service d'Aéronomie, CNRS/IPSL, 91371 Verrières le Buisson, France.*

Introduction:

This work presents stellar occultation data obtained by the SPICAM instrument (Spectroscopy for the Investigation of the Characteristics of the Atmosphere of Mars) onboard the Mars Express spacecraft. They have been collected for a period covering three quarter of a Martian year and represent the largest dataset on the structure of the Martian haze to date. It consists of 612 occultation sequences, with 500 of them successfully yielding haze profiles. Nearly all latitudes have been covered. Because these observations only require the faint light emitted by stars in the darkness, it allowed us to probe the deep Martian polar night, a region where hazes and the atmosphere in general are poorly documented. The UV-wavelength range covered by the SPICAM experiment is large and the resolution high enough so that constraints on the aerosol spectral behavior could be placed. Despite the variety of cases, we have attempted to summarize the behavior of hazes to derive some information of global nature. We specifically discuss aerosol profiles showing cloud features and give quantitative estimates of their properties. We have also focused on profiles collected in the polar night for which we have computed the haze opacity and its vertical distribution.

Data Presentation: The occultation technique relies upon the determination of atmospheric transmission at various heights above the surface. Only relative measurements are needed to infer species abundances, and thus the method is self-calibrated. Since SPICAM is not equipped with a pointing system, occultation sequences require a change of the spacecraft attitude so the instrument can sight a specific star and place it on the intensifier/CCD detector right in the central band. Along the orbital trajectory of Mars Express, the spacecraft maintains this attitude long enough to let a spectrum be acquired both from outside and through atmosphere. We consider the slant path to be outside the atmosphere when the tangential altitude is sufficiently high (usually several hundreds of km) so that absorbing species are so scarce they do not affect the appearance of the light source. This is the altitude range at which a reference spectrum of the star is obtained. The ratio of spectra taken through and outside the atmosphere gives an atmospheric transmission at each altitude above the point on the surface that is closest to the slant. If there is any absorbing or/and scattering species along the optical path between the star and

the spacecraft, photons are lost and resulting transmissions are lower than 1.

Method. The whole UV data inversion method was originally developed for the ENVISAT mission in order to retrieve NO_x species and temperature profiles in the Earth atmosphere from stellar occultation data (Hauchecorne et al., 2005). The adaptation to Mars is described in details elsewhere (Quémerais et al., 2005). The 118-320 nm spectral range covered by the UV channel bears the signature of CO₂, O₃ and aerosols (dust or/and cloud particles). Carbon dioxide and ozone have each a distinct absorption feature respectively shortward of 200 nm and around 250 nm. Aerosols contaminate the whole spectrum. We approximate their opacity as a function of wavelength using a formula commonly employed for terrestrial aerosols (Dubovik et al., 2000):

$$\tau_{\lambda} = \tau_{\lambda_0} (\lambda_0 / \lambda)^{\alpha} \quad (1)$$

where λ is the wavelength in nanometers, τ_{λ_0} is the aerosol slant opacity at a reference wavelength λ_0 (taken here at 250 nm) and α is commonly referred as to the Angström coefficient. Larger α values are usually indicative of particles smaller than the sampled wavelength (Dubovik et al., 2000). Instrumental noise causes a systematic uncertainty of about 5% in the retrieved quantities. The vertical profile of each species concentration is obtained with a standard "onion peeling" technique and a Tikhonov regularization to reduce numerical noise (Quémerais et al., 2005). Pressure profile is deduced from the vertical distribution of CO₂ density by integration of the hydrostatic equation. Temperature is then given by the ideal gas law. The altitude range of observations remains generally between 20 and 150 km. Above 150 km, atmospheric extinction is too weak to be detected at the 1- σ confidence level, whereas below 30 km, opacity of the Martian haze becomes progressively so thick that SPICAM does not detect any photon. With a measurement frequency of 1 Hz, the vertical resolution usually ranges from 1 to 3 km.

Results. Since the very first occultation sequence made on the 01/13/2004, more than 600 profiles have been collected by SPICAM. A number of sequences were lost due to pixel saturation, or a mispositioning of the star image on the detector. Some sequences were contaminated by stray light, and some were rejected due to a systematic anomalous spectrum behavior. At this point, almost five hundred sequences have been consistently treated and

yield vertical profiles of atmospheric species. The dataset spans a period comprised between the end of northern winter (at $L_s=330^\circ$, which corresponds to the arrival of Mars Express at Mars) and the northern winter solstice ($L_s=270^\circ$). As shown by Figure 1, a majority of observations have been performed in the southern hemisphere, and especially within three latitudinal annuli: 15, 30 and 75°S.

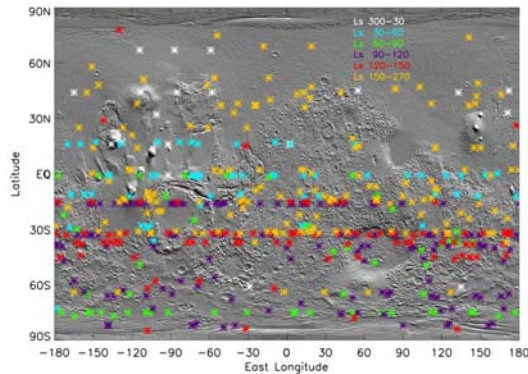


Figure 1: A MOLA-map of the Martian surface showing the locations of the Mars nearest point along the line of sight for all processed occultations. Color coding refers to the season of observation as indicated in the figure.

Seasonal signal: Jaquin et al. [1986] analyzed the seasonal variation of the maximum elevation at which aerosols are detected in the low-latitude regions. This study clearly shows that the Martian haze is keyed to seasons as its top gradually increases from aphelion ($L_s=70^\circ$) to perihelion ($L_s=250^\circ$). The same analysis has been conducted with our dataset, using a threshold value of 0.1 as the minimum aerosol slant opacity (at $\lambda=200$ nm) at which particles are considered present along the line of sight. Resulting seasonal variations of the hazetop as monitored by SPICAM are plotted in Fig. 2 which includes variations as a function of latitude. Our results corroborate previous Viking observations and show again strong variations of the Martian haze associated to seasons. However, what may appear related to the influence of the eccentric Martian orbit also reflects the effect of the spacecraft periapsis drifting latitudinally during the mission. Since the latter has consequences on the spatial sampling, the strong decrease of the hazetop around aphelion is also the result of the spacecraft periapsis progressively moving to the colder high latitude regions of the southern fall hemisphere. The following increase corresponds to a return into warmer equatorward latitudes. Thus differences in haze elevation are strongly correlated to thermal contrasts. This relation can be explained by two separate, yet combined, effects. First, with reduced insolation comes weaker convective activity and thus less capacity for the atmosphere to maintain particles higher up. Warmer re-

gions are therefore more prone to exhibit elevated hazetops. The second effect is the result of changes in the water condensation level. Since cloud particles form onto mineral dust aerosols, subsequent crystal fall scavenges dust to lower heights. This is why we usually see clouds sitting on top of the Martian haze as they set an upper limit above which dust hardly propagate. Temperature changes affect the altitude of cloud formation and subsequently modulate the elevation of the whole haze layer. This explains why the Martian haze is particularly sensitive to seasons.

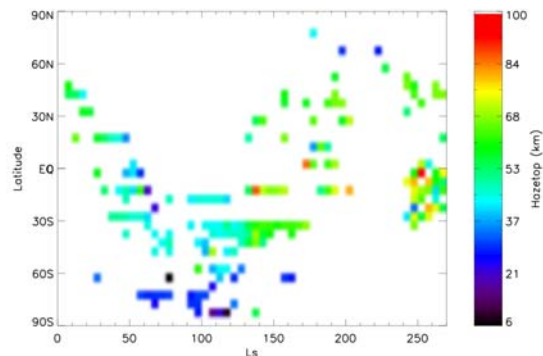


Figure 2: Seasonal variations of the hazetop as a function of latitude. Values have been averaged in boxes of 5° in L_s and 5° of latitude. Despite the uneven spatial coverage, it is perceptible that low-to-mid latitude regions experience a significant hazetop increase from aphelion to perihelion seasons. This trend is likely the result of a climatic asymmetry generated by the eccentric orbit of Mars.

Properties of the average Martian haze profile: Data have been averaged to yield representative haze profiles (displayed in Fig. 3) for two latitudinal sectors chosen for their distinct regimes: (a) between the equator and 15° and (b) poleward of 15° . Around the equator, the haze is more confined at lower heights and seems optically thicker. Opacity gradually decreases from bottom to top which suggests a dominant affect of sedimentation and mixing on the overall structure. The average Angström coefficient profile is roughly constant up to 55 km and then increases up to 80 km. Poleward of 15° , the haze is less confined and displays a prominent spike around 55 km, the likely result of recurrent cloud layers. Differences between the two latitudinal sectors are also noted for the Angström coefficients which are slightly shifted to higher values in the mid-to-high latitude profile, suggesting substantially smaller particles. The absence of upwelling motions as strong and as large as those encountered near the equator around solstices when the Hadley cells fully develop certainly factors in smaller particles dominating the haze structure above 25 km away from the equator. We have estimated the size of particles using a pre-computed equivalence-table between radius and Angström coefficient. As indicated in Fig. 3, the atmospheric region above 60 km is populated by sub-micronic particles ($r_{\text{eff}} < 0.1 \mu\text{m}$) at all latitudes. We interpret this feature as the presence of a background

population of very fine aerosols, probably dust, that are long-term stable at high altitude while micron-sized grains have been eliminated by sedimentation. Below 50 km near the equator, particle size can no longer be discriminated as sizes are probably larger than 0.3 μm in radius (the limit above which SPICAM spectral range makes it insensitive to detect changes in particle size). This is consistent with previous observations where a particle radius of 0.8 μm was inferred at 25 km in the equatorial region [Korablev et al., 1993].

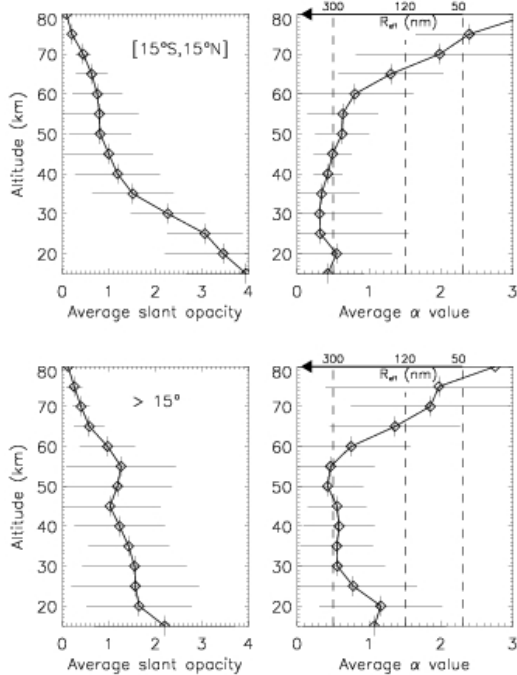


Figure 3-Upper plots: Opacity (left) and Angström coefficient (right) profiles obtained after averaging all occultation data inside 5 km atmospheric slices (shown by the small vertical bars assigned to each point). Profiles are representative of the near-equator region extending between 15°N and 15°S. Horizontal bars indicate the standard deviation of data from the average. The upper axis of the right-hand profile indicates the range of particle radius equivalent to that of the Angström coefficient on the lower axis. **Lower plots:** Same as above except for the regions poleward of 15° in both hemispheres.

Properties of detached layers: Statistics based on a visual inspection of profiles morphology reveals that more than 60% of occultation sequences exhibit at least one discrete layer probably of condensate origin, although a dust plume can not be excluded. Detached layers were also a common feature in Viking limb images [Jaquin et al., 1986]. We have selected a number of occultations where detached layers possess a well-defined structure and have used them for further analysis. Opacity profiles have been first processed through vertical inversion to obtain subsequent extinction profiles and then extinction coefficients have been integrated over the vertical extent of the detached layer to estimate the integrated cloud optical depth. For the sake of comparison with previous observations, optical depths have

been spectrally extrapolated from UV to visible wavelengths, using the Angström value to feed the α -model given in Eq. (1). All cloud characteristics are summarized in Table 1. Because SPICAM is blind below 20-30 km, our observations mostly sample clouds that form above 40 km. On the average, cloud opacity ranges from 0.01 to 0.1 in the UV and remains at about the same value in the visible since layers have a rather neutral spectral behavior. Cloud vertical thickness usually exceeds 10 km, reaching 30 km for the most vertically extended. Differences in cloud vertical extent likely track variations of convective strength, although no clear pattern could be drawn from our dataset. Corresponding Angström coefficients lie usually in a range where our retrievals lose sensitivity to particle size, which suggests ice crystal radii greater than 0.3 μm . We also distinguish several cases with a pronounced spectral behavior that can be robustly associated to a radius value of 0.1-0.2 μm .

where surface temperature falls below CO_2 condensation point during fall and winter. CO_2 condenses out on the ground and releases latent heat which balances cooling resulting from surface IR emission to space. This is one of the most remarkable phenomena of the Martian climate which is known to induce significant seasonal variations of the global pressure. Unfortunately, this aspect of Mars climate is incompletely documented. While atmospheric temperatures have been retrieved from IR measurements [Smith et al., 2001] and Radio occultations [Hinson et al., 2003], almost no information refers to aerosols except for one profile collected by TES near 80°N and discussed in Pearl et al. [2001]. Yet the abundance of aerosols in the polar nights is important

since they provide a source of diabatic cooling and possibly modifies the amount of condensing CO_2 . Subsequent affect of latitudinal thermal gradients could have consequences on the intensity of planetary-scale waves at mid-latitudes (J. Hollingsworth, personal communication). In addition, studies conducted in a theoretical framework have concluded on the possibility of CO_2 convective clouds associated with the rapid release of latent heat during atmospheric condensation episodes in the polar nights [Colaprete et al., 2003].

Occultations performed so far restrict our study to the south polar night. A subset of occultations has been further inverted to yield the vertical distribution of aerosol extinction (Fig. 4). These measurements exhibit a remarkably recurrent structure which differs significantly from profiles collected at other places on the planet. Polar nights are where SPICAM could access the lowest tangential altitudes (10 km and even below), implying that aerosols are both strongly confined and in low quantity. Most profiles exhibit a low hazetop (located around 30 km) and a monotoneous morphology wherein discrete layers are almost absent. Polar night temperature structure should provide a high degree of static stability, which then explains the observed low hazetop. Vigorous convective motions associated with CO_2 cloud

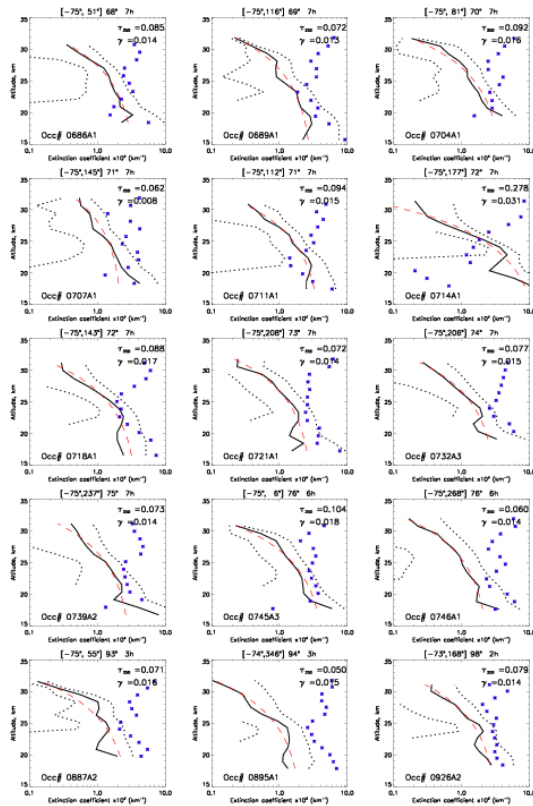


Figure 4: Aerosol extinction profiles (solid curves) computed from the vertical inversion of a selection of opacity profiles obtained in the polar night. Dotted curves indicate measurement uncertainties while blue crosses give the value of the Angström coefficient whose values suggest here the presence of particles smaller than $0.2 \mu\text{m}$ in radius. Red dashed curves show the vertical profiles of opacity obtained after fitting the data with a Conrath approximation (see text for explanation). Corresponding γ parameter are printed in the upper right corner. We also indicate the value of total UV opacity obtained from the vertical extrapolation of the fitted profile down to the surface.

formation are not necessarily ruled out but do not appear in our restricted statistics. The presence of suspended particles that deep in the polar night is interesting. Fig. 4 indicates that hazes are composed of particles with α values greater than 2. Such α values, consistent with a particle radius of no more than $0.1\text{--}0.2 \mu\text{m}$, are relatively high when compared to coefficients obtained at comparable altitude but in other regions. Polar night hazes are thus made of significantly smaller particles, suggesting that a specific microphysics is at work in this area. No spectral signature can be used to firmly conclude on their composition. Clouds are however believed to account for

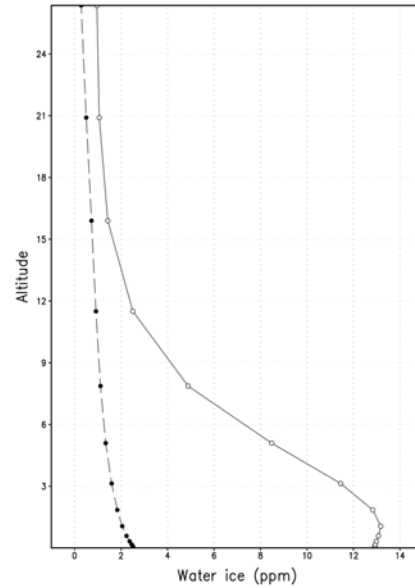


Figure 5: LMD-GCM predictions of water ice cloud profiles at 75°N (solid line) and 75°S (dashed line) respectively around northern winter solstice ($L_s 270^\circ$) and around northern summer solstice ($L_s 90^\circ$). North polar hood exhibits dramatically larger water ice content than its southern counterpart. However, both curves suggest a water ice haze declining continuously in the first 20 km of the atmosphere, in agreement with SPICAM observations.

the essential of the polar night haze, a statement supported by the only relevant TES limb profile spectrally identifying water ice as the unique haze component [Pearl et al., 2001]. In addition, climate models usually predict thick water ice clouds with a vertical structure similar to the one observed [Montmessin et al., 2004] (see Fig. 5 for the GCM profiles). If hazes observed by SPICAM were to be made of dust, then the particle size range estimated from data may indicate the presence of an Aitken core population which has escaped nucleation and further scavenging by clouds. Extrapolating haze profiles down to the surface, we estimate a typical column optical depth of about $0.05\text{--}0.1$ in the UV. The spectral behavior suggests the haze is probably a factor of 2 or 4 thinner at visible wavelengths. These estimations are obtained while attempting to fit profiles of extinction with the formula proposed by

Conrath [1975] to represent an aerosol profile in balance with sedimentation and mixing processes:

$$\sigma_z = \sigma_0 \exp[\gamma(1 - p_0/p_z)]$$

where σ is the extinction coefficient at 250 nm at a level p_z . σ_0 , the extinction coefficient at a reference level p_0 , and γ , the so-called Conrath parameter, are tentatively adjusted. As shown by Fig. 4, this representation proves particularly efficient at reproducing the typical structure of the polar night haze. γ is an important parameter for climate models which generally prescribe the dust vertical distribution according to Conrath's approximation. In order to help these models refine their prescription in the polar nights, we have performed additional fittings at a visible wavelength of 500 nm since most values for γ have been published in that range. We did this by extrapolating σ from 250 to 500 nm using the wavelength constraint placed by Angström coefficients. We obtain γ values around 0.03-0.05 (the higher γ , the shallower the dust layer). These values are slightly above that for typical weather conditions on Mars (0.03) confirming the higher vertical confinement of aerosols in the polar nights.

In short: Observations made by the SPICAM ultraviolet spectrometer onboard the Mars Express orbiter have yielded several hundreds of atmospheric profiles. These data are consistent with previous surveys of the Martian limb. The typical structure of the Martian haze possesses at least one discrete layer (60% of the cases) standing over an extended portion, the dusty layer, where opacity continuously increases down to the surface. Differences of morphology are however noted between profiles observed near the equator and profiles collected elsewhere. The Martian haze exhibits a pronounced seasonal signal manifested by variations of the maximum elevation at which particles are observed. For reasons related to both convective activity and changes in the hygropause level, cold regions display much lower hazetops than warm regions. Using UV spectrometry data, we put constraints on the haze microphysical properties. Vertical variations of particle size are keyed to variations of opacity. For instance, an increase of particle size is systematically noted near extinction peaks. This is the consequence of cloud formation which increases particle cross-section and size simultaneously. Despite marked differences of aerosol profiles between low and high latitudes, haze properties above 60 km are invariant, possibly reflecting the long-term presence of a background sub-micronic particle population. Several profiles have been analyzed in more details to extract the properties of detached cloud layers lofted above 40 km. Their total optical depth ranges from 0.01 to 0.1 in the visible. Estimation of cloud particle size is technically restricted due to SPICAM wavelength sampling but it agrees with a minimum radius value of about 0.3 μm while several estimates are consistent with a robust 0.1-0.2 μm . This crystal size, signifi-

cantly smaller than the 1 to 4 μm associated to recently classified type I and II clouds, suggests that a new class of clouds, henceforth type III clouds, can be extracted from our data. Observations made in the southern winter polar night indicate a very distinct aerosol behavior where particles are less abundant ($\tau < 0.1$), confined to low altitudes (consistent with a Conrath parameter exceeding 0.04) and made of particles with sizes on the order of 0.1 μm . This supports the idea that Martian polar nights are regions with a very clean atmosphere and a weak convective activity.

References:

- Colaprete, A., R. M. Haberle, and O. B. Toon, Formation of convective carbon dioxide clouds near the south pole of Mars, *Journal of Geophysical Research (Planets)*, 108 (E7), 17–1, doi:10.1029/2003JE002053, 2004.
- Conrath, B. J., Thermal structure of the Martian atmosphere during the dissipation of dust storm 1971, *Icarus*, 24, 34–46, 1975.
- Dubovik, O., A. Smirnov, B. N. Holben, M. D. King, Y. J. Kaufman, T. F. Eck, and I. Slutsker, Accuracy assessments of aerosol optical properties retrieved from Aerosol Robotic Network (AERONET) Sun and sky radiance measurements, *Journal of Geophysical Research*, 105 (14), 9791–9806, 2000JD900040, 2000.
- Hauchecorne, et al., First simultaneous global measurements of night time stratospheric NO₂ and NO₃ observed by Global Ozone Monitoring by Occultation of Stars (GOMOS)/Envisat in 2003. *Journal of Geophysical Research (Atmospheres)* 110 (D9), 18301–+, 2005.
- Hinson, D. P., R. J. Wilson, M. D. Smith, and B. J. Conrath, Stationary planetary waves in the atmosphere of Mars during southern winter, *Journal of Geophysical Research (Planets)*, 108 (E1), 4–1, 2002JE001949, 2003
- Jaquin, F., P. Gierasch, and R. Kahn, The vertical structure of limb hazes in the Martian atmosphere, *Icarus*, 68, 442–461, doi:10.1016/0019-1035(86)90050-3, 1986.
- Korablev, O. I., V. A. Krasnopolsky, A. V. Rodin, and E. Chassefiere, Vertical structure of Martian dust measured by solar infrared occultations from the PHOBOS spacecraft, *Icarus*, 102, 76–87, doi:10.1006/icar.1993.1033, 1993.
- Montmessin, F., F. Forget, P. Rannou, M. Cabane, and R. M. Haberle, Origin and role of water ice clouds in the Martian water cycle as inferred from a general circulation model, *Journal of Geophysical Research (Planets)*, 109 (E10), 100040, doi: 10.1029/2004JE002284, 2004.
- Pearl, J. C., M. D. Smith, B. J. Conrath, J. L. Bandfield, and P. R. Christensen, Observations of Martian ice clouds by the Mars Global Surveyor Thermal Emission Spectrometer: The first Martian year, *Journal of Geophysical Research*

(Planets), 106 (15), 12,325–12,338,
1999JE001233, 2001.

Quémerais, et al., *submitted to JGR (Planets)*

Smith, M. D., J. C. Pearl, B. J. Conrath, and P. R.
Christensen, Thermal Emission Spectrometer
results: Mars atmospheric thermal structure and
aerosol distribution, *Journal of Geophysical
Research (Planets)*, 106 (15), 23,929–23,945,
doi: 10.1029/2000JE001321, 2001.